AFG3L2 supports mitochondrial protein synthesis and Purkinje cell survival

Eva R. Almajan,[1] Ricarda Richter,[2] Lars Paeger,[1] Paola Martinelli,[1] Esther Barth,[1] Thorsten Decker,[2] Nils-Göran Larsson,[3,4] Peter Kloppenburg,[1,4,5] Thomas Langer,[2,3,4,5] and Elena I. Rugarli[1,4,5]

[1]Institute of Zoology and [2]Institute of Genetics, University of Cologne, Cologne, Germany. [3]Max Planck Institute for Biology of Ageing, Cologne, Germany. [4]Cologne Excellence Cluster on Cellular Stress Responses in Aging-Associated Diseases (CECAD) and [5]Center for Molecular Medicine, University of Cologne, Cologne, Germany.

Mutations in the *AFG3L2* gene have been linked to spinocerebellar ataxia type 28 and spastic ataxia-neuropathy syndrome in humans; however, the pathogenic mechanism is still unclear. *AFG3L2* encodes a subunit of the mitochondrial *m*-AAA protease, previously implicated in quality control of misfolded inner mitochondrial membrane proteins and in regulatory functions via processing of specific substrates. Here, we used a conditional *Afg3l2* mouse model that allows restricted deletion of the gene in Purkinje cells (PCs) to shed light on the pathogenic cascade in the neurons mainly affected in the human diseases. We demonstrate a cell-autonomous requirement of AFG3L2 for survival of PCs. Examination of PCs prior to neurodegeneration revealed fragmentation and altered distribution of mitochondria in the dendritic tree, indicating that abnormal mitochondrial dynamics is an early event in the pathogenic process. Moreover, PCs displayed features pointing to defects in mitochondrially encoded respiratory chain subunits at early stages. To unravel the underlying mechanism, we examined a constitutive knockout of *Afg3l2*, which revealed a decreased rate of mitochondrial protein synthesis associated with impaired mitochondrial ribosome assembly. We therefore propose that defective mitochondrial protein synthesis, leading to early-onset fragmentation of the mitochondrial network, is a central causative factor in AFG3L2-related neurodegeneration.

Introduction

Eukaryotic cells monitor the quality of their mitochondria using mechanisms acting at the interorganelle or intraorganelle level. Mitochondrial fusion and fission ensure maintenance of a functional network, whereas intramitochondrial proteases remove misfolded and aggregated proteins and also have a role in regulating mitochondrial function by processing specific substrates (1). Both levels of quality control are crucial in neurons, as emphasized by the increasing number of neurodegenerative diseases linked to impaired mitochondrial dynamics or mutations in mitochondrial proteases (1).

Subunits of the matrix ATPase associated with various cellular activities (*m*-AAA) protease have emerged as crucial players in defending neurons against neurodegeneration. The *m*-AAA protease is an evolutionary conserved hexameric complex in the inner mitochondrial membrane, exposing the catalytic domains to the matrix (2, 3). Studies in yeast and mammals have shown that the *m*-AAA protease degrades misfolded polypeptides and excess protein components lacking assembly partners in the inner mitochondrial membrane (2, 4, 5). Moreover, the yeast *m*-AAA protease mediates proteolytic maturation of the mitochondrial ribosomal component MRPL32 (6). MRPL32 maturation is a prerequisite for mitochondrial translation and the synthesis of mitochondrially encoded (mt-encoded) respiratory chain subunits, explaining respiratory deficiencies of yeast cells lacking the *m*-AAA protease (6). In a reconstituted yeast system, the mammalian *m*-AAA protease was able to process MRPL32, suggesting evolutionary conservation of this pathway (6).

In human mitochondria, the *m*-AAA protease is composed of 2 highly homologous subunits, paraplegin (encoded by the *SPG7* gene) and AFG3L2, which assemble to form hetero-oligomeric and, in the case of AFG3L2 only, homo-oligomeric functional complexes (7, 8). Heterozygous mutations in *AFG3L2* cause autosomal dominant spinocerebellar ataxia type 28, a neurological disorder clinically characterized by loss of balance, progressive gait and limb ataxia, and dysarthria, owing to degeneration of the cerebellum and its afferent and efferent connections (9). In contrast, a homozygous *AFG3L2* mutation (Y616C) has been found in 2 children from a consanguineous marriage affected by a severe, early-onset spastic ataxia-neuropathy syndrome, characterized by severe spasticity, ataxia, and myoclonic epilepsy (10). We showed that these patients carry a mutation that impairs the formation of homo-oligomers and, to an even greater extent, of hetero-oligomers within paraplegin, thus affecting the total amount of assembled *m*-AAA complexes (10). Remarkably, these patients showed a clinical phenotype that associates features of spinocerebellar ataxia with those of hereditary spastic paraplegia, a condition characterized by retrograde degeneration of axons of the cortical motoneurons. This is consistent with the finding that mutations in *SPG7*-encoding paraplegin cause autosomal recessive hereditary spastic paraplegia (11).

In both humans and mice, *AFG3L2* is expressed at high levels in all neurons, including Purkinje cells (PCs), while *SPG7* is enriched in large neurons, such as the pyramidal neurons of layer V of the cortex, spinal motor neurons, and PCs (9, 12). The different expression levels of the subunits and the ability to homo-oligomerize and/or hetero-oligomerize can affect the dosage of *m*-AAA isoenzymes in individual neurons and explain the specificity of the clinical phenotype when *AFG3L2* or *SPG7* are mutated. So far, there is no evidence for differential activities of hetero-oligomeric or homo-oligomeric *m*-AAA proteases, and the same molecular mechanism could underlie neuronal death

Conflict of interest: The authors have declared that no conflict of interest exists.
Citation for this article: *J Clin Invest.* 2012;122(11):4048–4058. doi:10.1172/JCI64604.

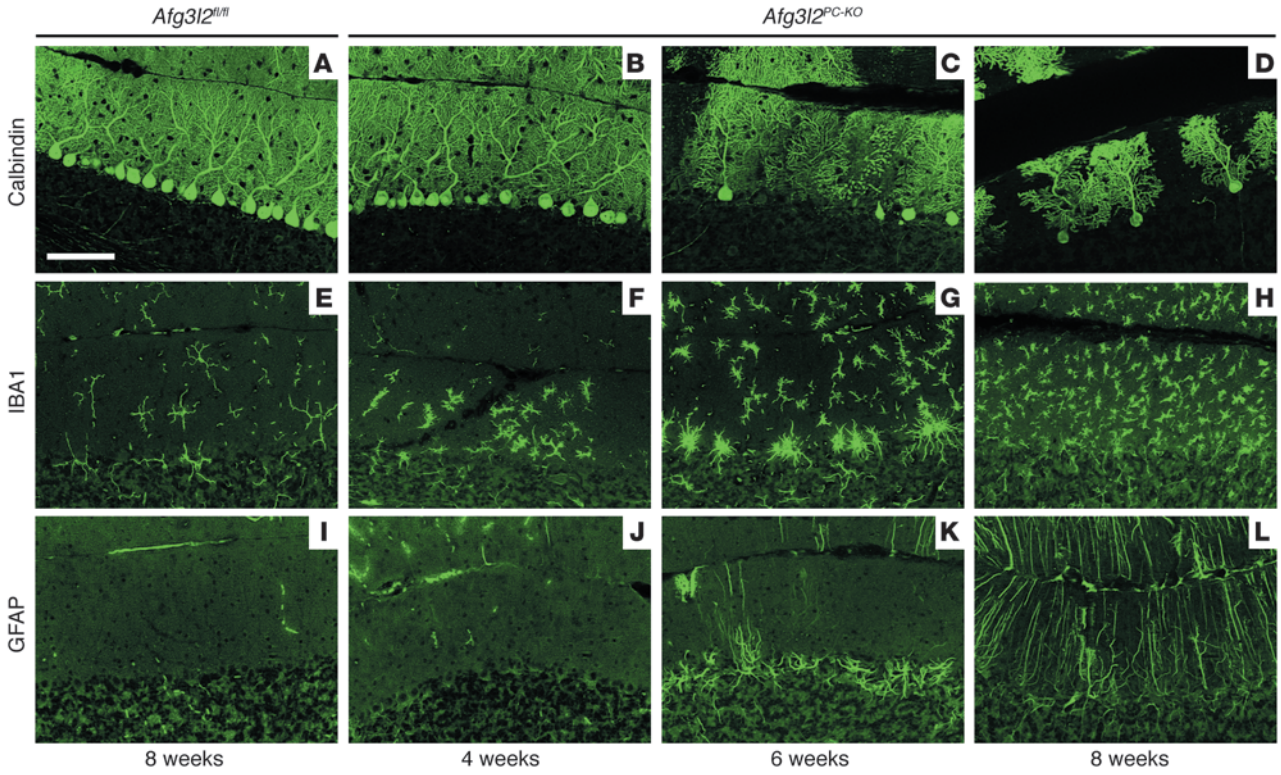

Figure 1
PCs degenerate over time in *Afg3l2*$^{PC–KO}$ mice. Vibratome sections of the cerebellum were collected at various time points from *Afg3l2*$^{fl/fl}$ and *Afg3l2*$^{PC–KO}$ mice and stained for (**A**–**D**) calbindin to show progressive PC loss, (**E**–**H**) IBA1 to detect resting and activated microglia, and (**I**–**L**) GFAP to mark reactive astrocytes. Scale bar: 100 μm.

in different areas of the central nervous system. Unraveling this mechanism is therefore crucial for a better understanding of the pathogenesis of the human diseases.

Afg3l2-deficient or -haploinsufficient mice have been recently described (13, 14). Mice lacking AFG3L2 are characterized by severe tetraparesis and early-onset lethality, associated with widespread impairment of axonal development and myelination in both central and peripheral nervous systems (13), while heterozygous mice show a late-onset cerebellar degeneration (14). Mitochondria isolated from these mice showed impaired ATP synthesis and reduced assembly of respiratory complexes I and III, although the underlying mechanism was not clarified (13, 14). In addition, AFG3L2-deficient mitochondria showed enhanced degradation of OPA1, the GTPase required for inner mitochondrial membrane fusion (15). Proteolysis is mediated by activation of another mitochondrial protease in the inner membrane, OMA1, and disrupts the balance between long and short OPA1 isoforms required for mitochondrial fusion (15). As a result, mouse embryonic fibroblasts isolated from *Afg3l2*-deficient mice showed a fragmented mitochondrial network when cultured under oxidative conditions (15). Whether this occurs also in affected neurons in vivo and has any role in mediating neurodegeneration is currently unknown. A previous study strongly indicated that PCs are particularly sensitive to impaired mitochondrial fusion (16).

Here, we used a conditional knockout of *Afg3l2* to specifically delete the gene postnatally in murine PCs, the main target of neurodegeneration in spinocerebellar ataxia. Our results demonstrate that AFG3L2 is required cell autonomously for survival of these neurons in adult life and that inflammatory changes occur secondarily. Moreover, we found that alterations of the mitochondrial network and cytochrome *c* oxidase (COX) deficiency are early events in affected neurons and are rapidly followed by cell death. Finally, we found a reduced rate of protein synthesis and mitochondrial ribosome (mitoribosome) assembly in brain mitochondria from an *Afg3l2* constitutive knockout. We therefore propose that lack of AFG3L2 directly affects mitochondrial protein synthesis, resulting in a very early alteration of the distribution and morphology of the mitochondrial network, followed by respiratory incompetence and cell death.

Results

PC-specific Afg3l2 deletion causes neurodegeneration and secondary inflammation. We developed a conditional mouse model in which the *Afg3l2* locus was modified with the insertion of 2 loxP sites flanking exons 4 and 5 (*Afg3l2*$^{fl/fl}$ mice) (Supplemental Figure 1; supplemental material available online with this article; doi:10.1172/JCI64604DS1). Upon Cre recombinase–mediated excision of these exons, a frameshift mutation leading to a premature stop codon was obtained. By allowing spatially and temporally controlled deletion of the *Afg3l2* gene, this strategy permits examination of the cell-autonomous role of *Afg3l2* in adult neurons.

We decided to specifically knockout the gene in adult PCs. These neurons are the main target of neurodegeneration linked to mutations in *AFG3L2* (9, 10) and express high levels of the gene

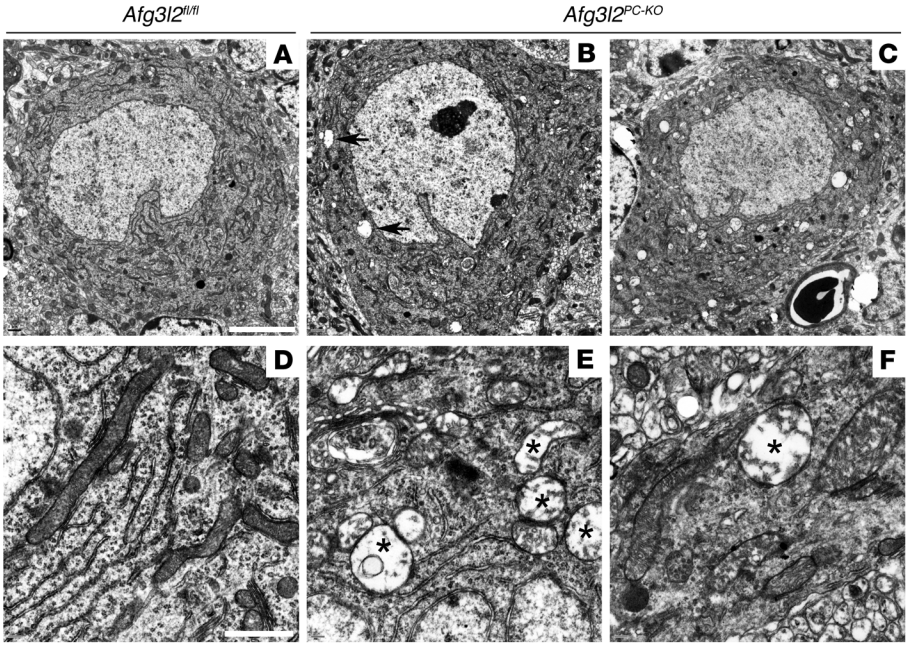

Figure 2
Ultrastructural analysis of PCs in *Afg3l2*$^{PC–KO}$ mice. (**A**) Electron micrographs of cerebella from 4-week-old mice show normal PCs in *Afg3l2*$^{fl/fl}$ mice. PCs in *Afg3l2*$^{PC–KO}$ mice appear grossly normal but display (**B**) a few (arrows) or (**C**) rarely many abnormal mitochondria in the cell body. Swollen mitochondria with disrupted cristae (labeled with asterisks) are present in (**E**) the cell body and (**F**) dendrites of PCs in *Afg3l2*$^{PC–KO}$ mice, (**D**) while normal mitochondria are present in the controls. White scale bars: 5 μm (**A**–**C**); 1 μm (**D**–**F**).

(9, 12). We crossed *Afg3l2*$^{fl/fl}$ mice with the L7-Cre transgenic line, which drives expression of the Cre recombinase specifically in PCs between 2 and 3 weeks of age (17) (Supplemental Figure 2). Homozygous *Afg3l2*$^{fl/fl}$ mice carrying the L7-Cre allele (referred to herein *Afg3l2*$^{PC–KO}$) were born at the expected ratio, were viable, and appeared normal. However, at about 8 weeks, they began to show unsteady gait in the cage. Histological examination of the cerebella from these mice showed dramatic degeneration of PCs over time (Figure 1). Prominent loss of PCs was observed at 6 weeks and progressed with time, leading to disappearance of almost all the neurons at 12 weeks (Figure 1, A–D, and Supplemental Figure 3). Calbindin staining of PCs indicated a normal number and appearance of the neurons and their dendritic trees at 4 weeks of age (Figure 1B). However, in some areas of the cerebellum at this time point, we observed an obvious switch of microglia, the resident immune cells of the brain, from a resting morphology, characterized by a small soma with many thin ramified processes, to an activated phenotype with cellular hypertrophy and retraction of cytoplasmic processes (Figure 1F). Reactive microglia promoted an inflammatory response that further engages the immune system (Figure 1, G and H) and stimulates reactive astrocytosis. In fact, Bergmann glial cells appeared hypertrophic in the PC layer at 6 weeks and in the molecular layer at 8 weeks (Figure 1, I–L). In conclusion, removal of AFG3L2 from PCs induces cell-autonomous neurodegeneration associated with secondary inflammatory response.

Distribution and morphology of the mitochondrial network are affected at early stages in Afg3l2$^{PC–KO}$ *mice*. Since neurodegeneration occurs postnatally and is progressive, the *Afg3l2*$^{PC–KO}$ model allows investigation of initial pathogenic steps. The presence of activated microglia surrounding morphologically normal PC bodies, starting at 4 weeks of age in *Afg3l2*$^{PC–KO}$ mice, prompted us to select this time point for further analysis. As a first step, we examined the ultrastructure of PCs by electron microscopy. PCs were easily identified by their large cell body and their alignment in a single layer. They contained several tubular mitochondria, often in close proximity to the endoplasmic reticulum in control mice (Figure 2, A and D). In *Afg3l2*$^{PC–KO}$ mice, overall PCs appeared normal, without visible signs of apoptotic or necrotic features. However, several PCs (9 out of 15 cells, from 3 mice) contained some swollen mitochondria, easily recognizable for their larger size, dilution of the matrix, and dramatic displacement to the periphery of the organelle of the cristae, which appeared shortened, reduced in number, and disorganized (Figure 2, B and E). Abnormal mitochondria were identified in both dendrites and axons of PCs (Figure 2F, data not shown). A PC filled with abnormal mitochondria was identified at 4 weeks of age (1 out of 15 cells) (Figure 2C).

These findings strongly suggest that alterations of the mitochondrial network occur in neurons lacking *Afg3l2* at an early stage. To image mitochondrial morphology and distribution in vivo, we used a reporter mouse in which the expression of yellow fluorescent protein (YFP) targeted to the mitochondrial matrix (mt-YFP) can be activated upon Cre excision (ROSA26$^{+/SmY}$ mice) (18). Previous analysis of these mice demonstrated that transgenic expression of the mt-YFP cassette does not interfere with mitochondrial function and morphology in vivo (18). We therefore imaged mt-YFP expression in *Afg3l2*$^{PC–KO}$ mice (*Afg3l2*$^{fl/fl}$;L7-Cre;ROSA26$^{+/SmY}$ mice) compared with that in control mice (*Afg3l2*$^{+/+}$;L7-Cre;ROSA26$^{+/SmY}$ or *Afg3l2*$^{+/–}$;L7-Cre;ROSA26$^{+/SmY}$ mice) at 4 weeks of age. Strong mitochondrial YFP expression was observed selectively in PC bodies and dendrites, as observed by concomitant calbindin staining (Supplemental Figures 2 and 4). No difference was observed in PCs of *Afg3l2*$^{+/+}$ and *Afg3l2*$^{+/–}$ mice (data not shown). They contained a dense network of mitochondria both in the cell body and in the dendritic tree. Tubular mitochondria positioned parallel to the main axis almost completely filled the dendrites in these animals (Figure 3, A and C, and Supplemental Figure 4). In *Afg3l2*$^{PC–KO}$ mice, the mitochondrial network showed initial signs of fragmentation at 4 weeks instead (Figure 3, B and D). Careful examination of the dendritic tree showed that, in several neurons, mitochondria did not fill the dendrite cytoplasm but appeared less abundant, clustered, and aggregated (Figure 3B). The fragmentation of the mitochondrial

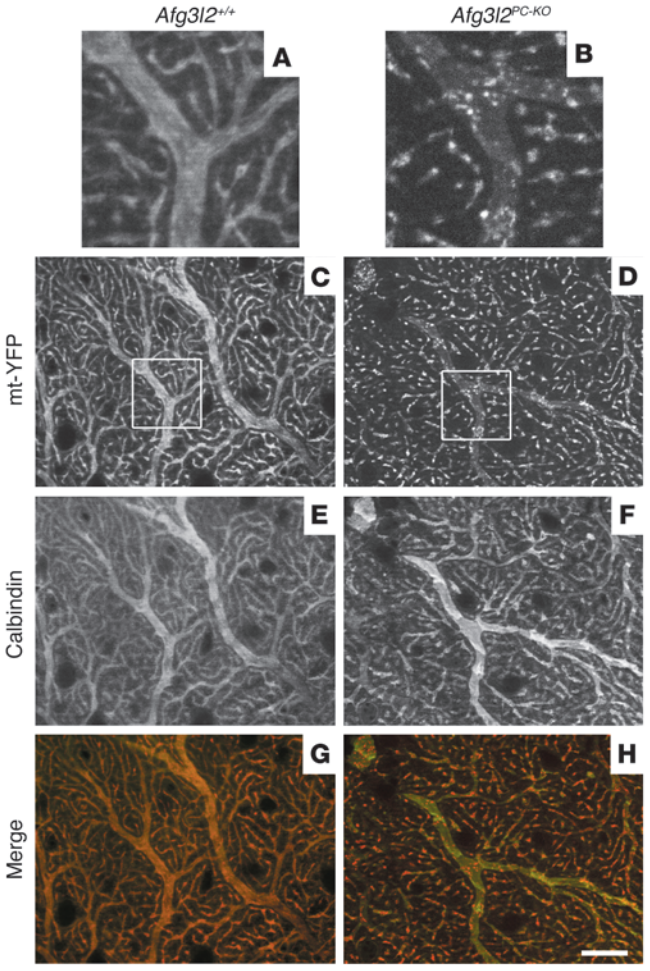

Figure 3
Abnormal mitochondrial network in *Afg3l2*$^{PC–KO}$ mice. Analyses were performed in animals of the shown genotypes crossed with ROSA26$^{+/SmY}$ mice. (**A**–**D**) The mitochondrial network is labeled with mt-YFP, (**E** and **F**) while PC dendrites are decorated using an antibody against calbindin. (**G** and **H**) In merged images, pseudocolors were used: calbindin is in green, while mt-YFP is in red. Images in **A** and **B** show enlarged views of the boxes in **C** and **D**, respectively. (**C**) mt-YFP expression in control mice shows an elongated network of mitochondria (**E** and **G**) that follows the pattern of PC dendrites labeled with calbindin, (**A**) with mitochondria filling the entire space of large caliber dendrites. (**D**) In *Afg3l2*$^{PC–KO}$ mice, the mitochondrial network shows initial fragmentation, with (**B**, **F**, and **H**) some large-caliber calbindin-stained dendrites depleted of mitochondria, which appear clustered. Scale bar: 20 μm.

network was very pronounced at 6 weeks in degenerating PCs (Supplemental Figure 4).

We then asked whether fragmentation and clustering of mitochondria in otherwise morphologically normal PCs affect the electrophysiological properties of these neurons. PCs in brain slices of 4- to 5-week-old *Afg3l2*$^{PC–KO}$ mice and their control littermates were recorded under current clamp, using the perforated patch clamp configuration to ensure the integrity of intracellular components. PCs were identified by their YFP fluorescence. After the electrophysiological characterization, the PCs were labeled by dye injection via the recording electrode. All parameter values that we determined for the electrophysiological properties of control PCs (Figure 4) were well in the range that has been described previously for PCs in rat and mouse brain slices and in vivo preparations (19–24). The statistical comparison of these electrophysiological parameters between PCs of *Afg3l2*$^{PC–KO}$ mice and their control littermates revealed no differences (Figure 4). PCs in both genotypes had no spontaneous activity or fired action potentials with high frequencies (Table 1). The tight inter-spike interval distributions reflected the regular firing frequency in both genotypes, with no differences in spike waveform (Figure 4C and Table 1). Further electrophysiological parameters that we analyzed were not different between silent and spiking PCs, and all data were pooled for each genotype. PCs of both genotypes had similar input resistances and responded to hyperpolarization with a characteristic sag-like, slowly developing inward rectification (Figure 4, A and B, and Table 1). Taken together, these results indicate that alterations in mitochondrial network occur at early stages of the disease, before changes in the electrophysiological properties of cerebellar PCs become apparent.

AFG3L2-deficient PCs show respiratory dysfunction. The previous data indicate that the lack of AFG3L2 in PCs induces an early alteration of the mitochondrial network, which precedes overt signs of degeneration and impairment of electrophysiological function. Respiratory dysfunction is known to trigger OPA1 degradation and mitochondrial fragmentation (25, 26). This degradation is mediated by the protease OMA1 (15, 27), which can also be activated in absence of overt respiratory defects in mouse embryo fibroblasts (MEFs) with downregulated *Afg3l2* in vitro (15). We therefore decided to monitor respiratory function in PCs in vivo, using histochemical techniques to simultaneously analyze the enzymatic activity of COX and succinate dehydrogenase (SDH) in situ. COX is encoded by both nuclear and mitochondrial DNA (mtDNA), while SDH is exclusively nuclear encoded. A combined COX-SDH staining is therefore helpful to detect respiratory deficits associated to defects in mt-encoded subunits of the respiratory chain. In control mice, all PCs showed a dark brown staining, consistent with positive COX and SDH double staining (Figure 5). Surprisingly, in *Afg3l2*$^{PC–KO}$ mice, 9.8% ± 0.96% of PCs appeared blue, owing to severe COX deficiency associated with normal SDH activity. This percentage of respiratory deficient neurons is in agreement with the number of neurons showing dramatic mitochondrial defects observed in ultrastructural analysis. Notably, we did not observe an increase in the percentage of COX-negative, SDH-positive PCs at 6 weeks of age, strongly suggesting that neurons die shortly after manifesting this phenotype.

Mitochondrial protein synthesis is impaired in the brains of Afg3l2$^{Emv66/Emv66}$ *mice*. Several explanations can underlie the findings of COX-negative but SDH-positive PCs in *Afg3l2*$^{PC–KO}$ mice. Lack of AFG3L2 can affect mtDNA stability, mitochondrial gene expression, and/or mitochondrial translation. Since the PC-specific knockout does not allow in-depth biochemical analyses, we examined the constitutive *Afg3l2*$^{Emv66/Emv66}$ mouse to distinguish among these possibilities. This mouse carries a retroviral insertion in intron 14 of *Afg3l2*, resulting in lack of expressed protein (13). *Afg3l2*$^{Emv66/Emv66}$ mice die at approximately 2 weeks and show a generalized defect in axonal development (13). In the cerebellum, the number of PCs is not affected, but these neurons fail to develop a dendritic tree (12). We first examined mtDNA levels by real-time PCR. No significant differences were detected between

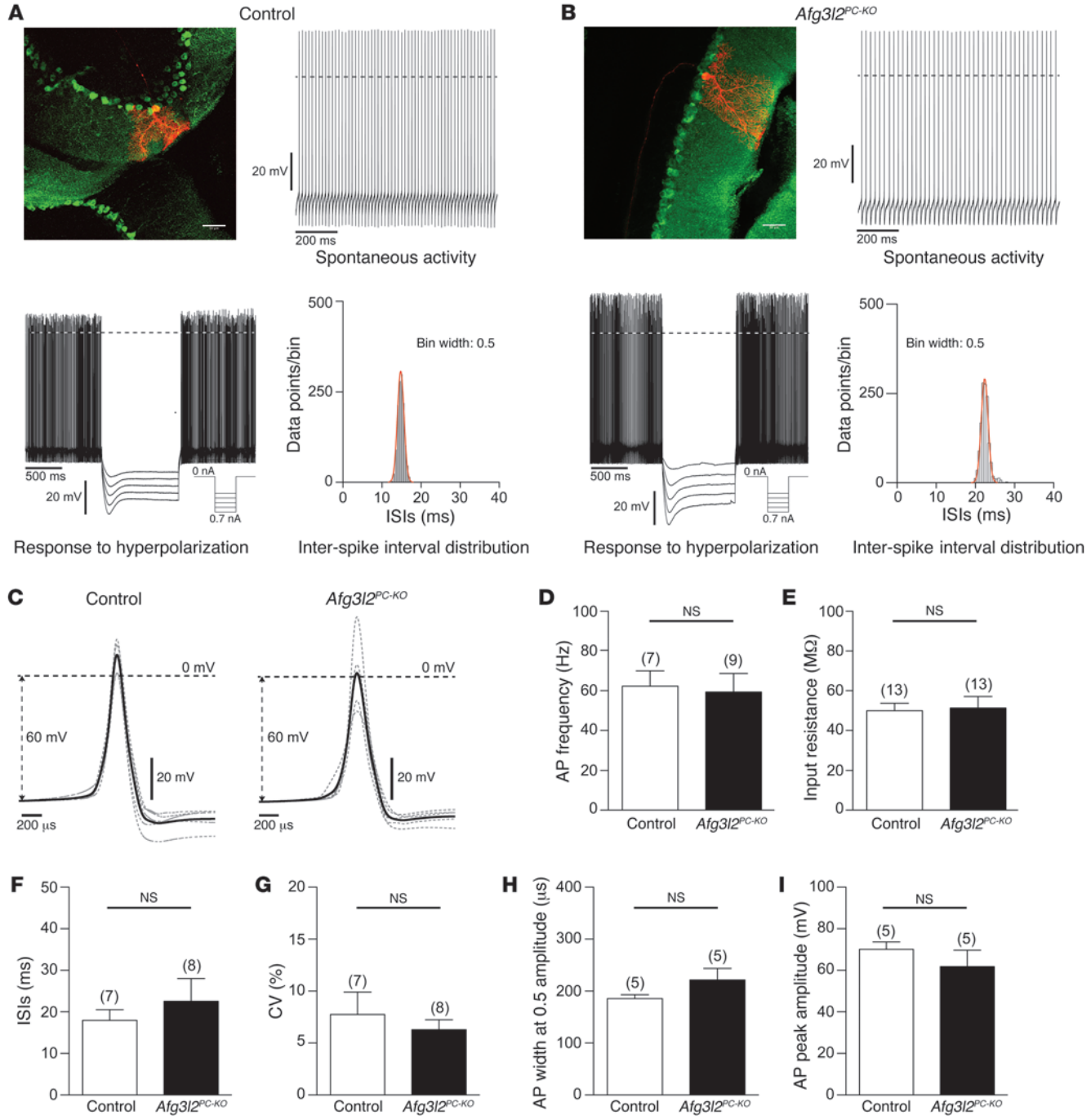

Figure 4

Electrophysiological properties of PCs in 4- to 5-week-old *Afg3l2*$^{PC–KO}$ mice and control littermates. PCs were recorded in the perforated patch clamp configuration and labeled with biocytin/streptavidin after the electrophysiological characterization. (**A** and **B**) Fluorescence images and electrophysiological data of (**A**) control and (**B**) *Afg3l2*$^{PC–KO}$ mice. Scale bars: 50 μm. The graphs show examples of the spontaneous activity and the inter-spike interval distributions during spontaneous activity and the membrane potential in response to hyperpolarizing current injections. Hyperpolarization induced a sag-like, slowly developing inward rectification. Dashed lines mark the 0-mV border. (**C**) PC action potential waveforms of control and *Afg3l2*$^{PC–KO}$ mice. The average of all neurons is shown in bold black. The average of individual neurons is shown in gray. (**D**) Membrane potential, (**E**) input resistance, (**F**) inter-spike interval (ISI), (**G**) coefficients of variance (CV) of the inter-spike interval distributions, (**H**) action potential (AP) width at 0.5 maximal amplitude, and (**I**) action potential maximal amplitude of control and *Afg3l2*$^{PC–KO}$ mice. Numbers over bars indicate the number of neurons. Error bars show SD.

Table 1
Electrophysiological properties of *Afg3l2*$^{PC\text{-}KO}$ PCs at 4 to 5 weeks of age

	Control	*Afg3l2*$^{PC\text{-}KO}$	*P* value
No spontaneous activity	6 out of 13 neurons	4 out of 13 neurons	
Spike frequency	62 ± 8 Hz (*n* = 7 out of 13)	60 ± 9 Hz (*n* = 9 out of 13)	0.82
Inter-spike interval	18 ± 3 ms (*n* = 7)	23 ± 5 ms (*n* = 8)	0.48
Inter-spike interval distributions (coefficient of variance)	8% ± 2% (*n* = 7)	6% ± 1% (*n* = 8)	0.48
Spike width at 0.5 maximal amplitude	186 ± 7 μs (*n* = 5)	221 ± 22 μs (*n* = 5)	0.16
Spike peak amplitude	70 ± 4 mV (*n* = 5)	62 ± 8 mV (*n* = 5)	0.36
Input resistance	50 ± 4 MΩ (*n* = 13)	51 ± 6 MΩ (*n* = 13)	0.85

Afg3l2$^{Emv66/Emv66}$ and control littermates at 10 days of age (Figure 6A). We therefore concluded that loss of AFG3L2 does not affect mtDNA stability. We then performed Northern blot analysis to evaluate the steady-state levels of a number of mt-encoded mRNAs. We did not detect significant differences in expression of *Cox1*, *Cox3*, cytochrome b (*Cytb*), NADH dehydrogenase subunit 1 (*Nd1*), and the mitochondrial ribosomal RNA 16S (*Rnr2*) between *Afg3l2*$^{Emv66/Emv66}$ and control littermates (Figure 6B).

Lack of AFG3L2 may affect mitochondrial protein synthesis. To directly address this possibility, we isolated mitochondria from the brains of control and *Afg3l2*$^{Emv66/Emv66}$ mice and monitored the rate of mitochondrial protein synthesis rate in organello after incorporation of ^{35}S-Met in de novo synthesized proteins. Mitochondrial translation was severely impaired in mitochondria isolated from the brains of *Afg3l2*$^{Emv66/Emv66}$ animals compared with that in wild-type littermates (Figure 6C). Remarkably, a similar phenotype was observed in liver mitochondria (Supplemental Figure 5). We excluded that mitochondrial fragmentation per se impairs mitochondrial protein synthesis (Supplemental Figure 6).

Given these data, we analyzed the steady-state levels of mt- or nuclear-encoded subunits of respiratory complexes. A reduction of the steady-state levels of mt-encoded subunits of complex I (ND2), complex III (CYTB), and complex IV (COX1 and COX3) was observed, while the levels of the nuclear-encoded COX4 or NDUFA9 were unaffected (Figure 6D). This finding is in line with the reduction of assembled respiratory complexes I and III that was previously reported in *Afg3l2*$^{Emv66/Emv66}$ mitochondria (13). In addition, we also found that respiratory complex IV assembles at reduced levels (Supplemental Figure 7). These findings demonstrate that AFG3L2 deficiency is associated with an impairment of mitochondrial translation and provide an explanation for the COX deficiency that we observed in *Afg3l2*-deficient PCs.

Defective assembly of the mitoribosome in Afg3l2$^{Emv66/Emv66}$ *mice.* To further define the molecular basis for the observed translation defect, we examined the assembly of mitoribosomes in *Afg3l2*$^{Emv66/Emv66}$ mice. A sedimentation analysis of mitochondrial extracts from the brains and livers of *Afg3l2*$^{Emv66/Emv66}$, *Afg3l2*$^{Emv66/+}$, and control littermates revealed reduced levels of assembled mitoribosomes in *Afg3l2*$^{Emv66/Emv66}$ mice (Figure 7A and Supplemental Figure 5). Mitochondrial ribosomal proteins L12, L13, and L32 (MRPL12, MRPL13, and MRPL32), which are subunits of the large 39S mitoribosomal particle (mt-LSU), relocated to less dense fractions in *Afg3l2*$^{Emv66/Emv66}$ mice compared with both heterozygous and controls. MRPL12 and MRPL32 were also found at the top of the gradient, likely representing free protein. Notably, the amount of MRPL32 appeared reduced in *Afg3l2*$^{Emv66/Emv66}$ mitochondria. We therefore further examined the steady-state levels of this and other ribosomal subunits (Figure 7B). In *Afg3l2*$^{Emv66/Emv66}$ mice, we found markedly decreased steady-state levels of MRPL32 in the brain and in several other tissues (Figure 7C). However, we could not reproducibly detect an accumulation of the precursor of MRPL32, probably owing to increased degradation. In contrast, the steady-state levels of other subunits of the mitoribosome were not visibly affected by lack of AFG3L2 (Figure 7B). In conclusion, these data indicate that AFG3L2 deficiency affects the biogenesis of the mt-LSU, leading to reduced assembly of the mitoribosomes.

Discussion

The role of the *m*-AAA protease in neurodegeneration has emerged in recent years, with the identification of 3 different neurodegenerative conditions linked to mutations in paraplegin or AFG3L2 (9–11). However, it has been difficult to pinpoint the pathogenic pathway underlying these diseases, owing to the broad range of activities performed by the *m*-AAA protease in mitochondria (1). Here, we show that lack of AFG3L2 in neurons affects mitoribosome assembly and mitochondrial translation, leading to very early changes in the mitochondrial network and finally to cell-autonomous cell death.

We provide evidence that AFG3L2 is required autonomously in PCs to protect against degeneration. Remarkably, 3 weeks after establishment of Cre recombinase expression in PCs, a large number of neurons lacking AFG3L2 are lost, suggesting that AFG3L2 is required for neuronal survival. This is consistent with the high level of AFG3L2 expression and its presence in all isoenzymes of the *m*-AAA protease (8, 12). The vulnerability of PCs to deficiency of the *m*-AAA protease is in agreement with previous findings, showing that these neurons are a preferential target when mitochondrial function is affected (16, 28, 29). Our data also show that the inflammatory responses already observed in heterozygous

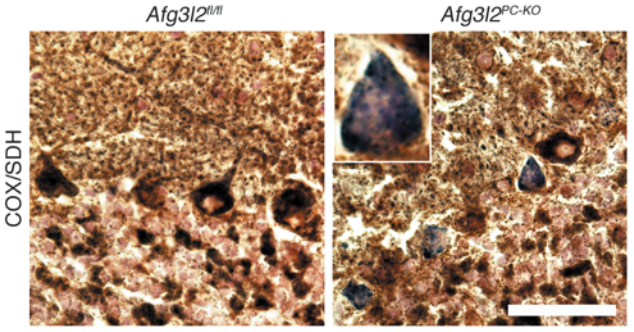

Figure 5
Afg3l2$^{PC\text{–}KO}$ mice show COX-deficient PCs. Combined COX-SDH enzymatic staining at 4 weeks of age reveals normal brown PCs in control mice, while several PCs stain blue in the *Afg3l2*$^{PC\text{–}KO}$ mice, indicating COX deficiency. Scale bar: 200 μm.

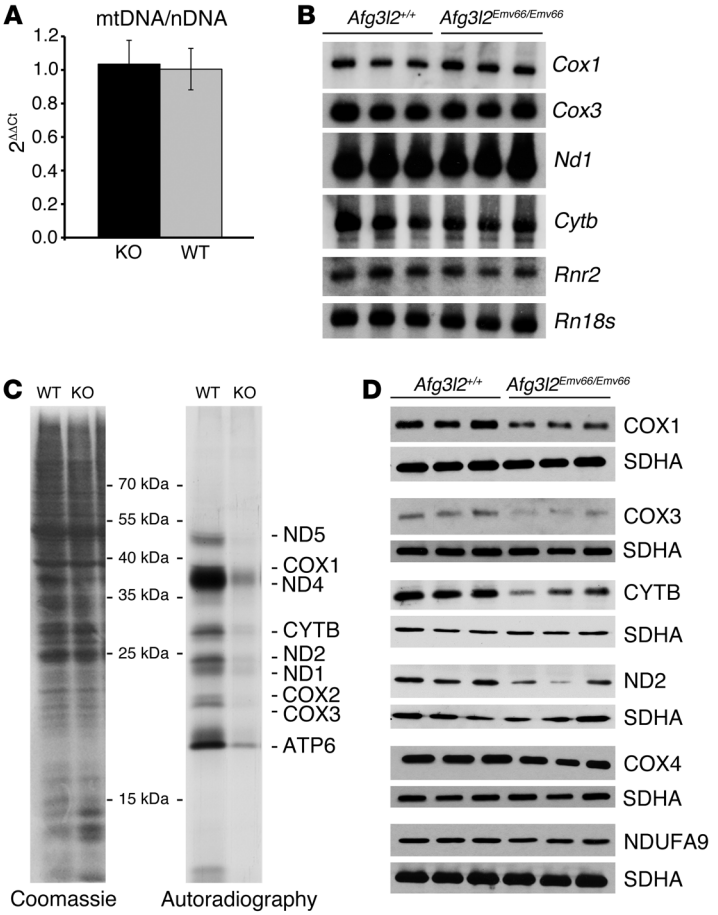

Figure 6
Impaired mitochondrial protein synthesis in brain mitochondria from *Afg3l2*$^{Emv66/Emv66}$ mice. (**A**) Real-time PCR quantification shows no statistically significant difference of the mtDNA content with respect to the nuclear DNA (nDNA) in the brains of *Afg3l2*$^{+/+}$ (WT) and *Afg3l2*$^{Emv66/Emv66}$ (KO) mice. Error bars show SD. (**B**) Northern blot analysis of a subset of mitochondrial transcripts reveals similar levels of expression in the brains of *Afg3l2*$^{+/+}$ and *Afg3l2*$^{Emv66/Emv66}$ mice. 18S RNA (*Rn18s*) was used as loading control. (**C**) In organello translation after labeling with ^{35}S-met shows reduced de novo synthesized protein levels in *Afg3l2*$^{Emv66/Emv66}$ mice when compared with those in *Afg3l2*$^{+/+}$ mice. Coomassie brilliant blue staining of the gel shows equal loading of proteins. (**D**) The steady-state levels of mt-encoded COX1, COX3, CYTB, and ND2 are reduced in the brains of *Afg3l2*$^{Emv66/Emv66}$ mice compared with those in *Afg3l2*$^{+/+}$ mice, while levels of nuclear-encoded COX4 and NUDFA9 appear unaffected. The SDHA subunit of complex II was used as loading control.

Afg3l2 mice (14) are secondary to loss of PCs, as observed in several other neurodegenerative conditions (30). Bergmann glial cells are unipolar astrocytes located around the soma of PCs, which extend smooth radial fibers to the pial surface. These processes direct the growth of PC dendrites, with which they maintain a close functional relationship during life (31). These cells become hypertrophic and express increased levels of glial fibrillary protein (GFAP), in parallel with the progressive degeneration of PCs. In addition, we found a clear switch of microglial cells from the ramified morphology typical of resting cells to an activated morphology (32). This switch occurs as early as 4 weeks of age, before any morphological or functional sign of neurodegeneration can be detected, consistent with the active role of these cells as efficient sensors of pathologic states (32).

The conditional model for *Afg3l2* deficiency has the great advantage of allowing examination of neurons at a very early stage of the degenerative process. This time point helped us distinguish pathologic processes that occur upstream, as a direct consequence of lack of the gene, from later secondary events. Our analysis provides evidence that fragmentation and abnormal distribution of mitochondria occur in PCs at very early stages and precede neurodegeneration, indicating that they are not the result of the neurodegenerative process but contribute to the pathogenic cascade. Remarkably, these alterations occur at early stages when the electrophysiological function of the neurons is still normal. We previously showed that in *Afg3l2*-deficient MEFs the protease OMA1 is activated and mediates stress-induced cleavage of long OPA1 isoforms, thereby inhibiting mitochondrial fusion (15). The current data indicate that this process is relevant in vivo for the neurons affected in spinocerebellar ataxia. Abnormalities in mitochondrial fusion were already suggested to contribute to PC degeneration and COX deficiency in a conditional mitofusin-2 (MFN2) mouse model crossed with the L7-Cre transgenic line (16). However, in case of MFN2 deletion, the progression of the phenotype was slower than that in our model (residual PCs were still present at 3 months), and lack of fusion was associated with loss of mtDNA (16). In contrast, mtDNA stability was not affected in *Afg3l2*$^{Emv66/Emv66}$ mice, while, already, at 4 weeks, almost 10% of PCs displayed COX deficiency but normal SDH staining.

Abnormalities of the mitochondrial network and COX deficiency could be two concomitant but independent events, since we previously found that downregulation of the *m*-AAA protease in MEFs can lead to fragmentation of the mitochondrial network without respiratory deficiency (15). However, absence of AFG3L2 in vivo affects the respiratory function of PCs, and this could lead to OPA1-dependent fragmentation of the mitochondrial network, which in turn contributes to the pathogenic cascade. Moreover, we are probably underestimating the degree of respiratory impairment, since histochemical stainings can detect enzymatic activity even when this is below the normal range (33).

We demonstrate for what we believe to be the first time that lack of AFG3L2 affects the rate of mitochondrial translation and the steady-state levels of mt-encoded respiratory chain subunits in the brain of a constitutive *Afg3l2* knockout. The mitochondrial

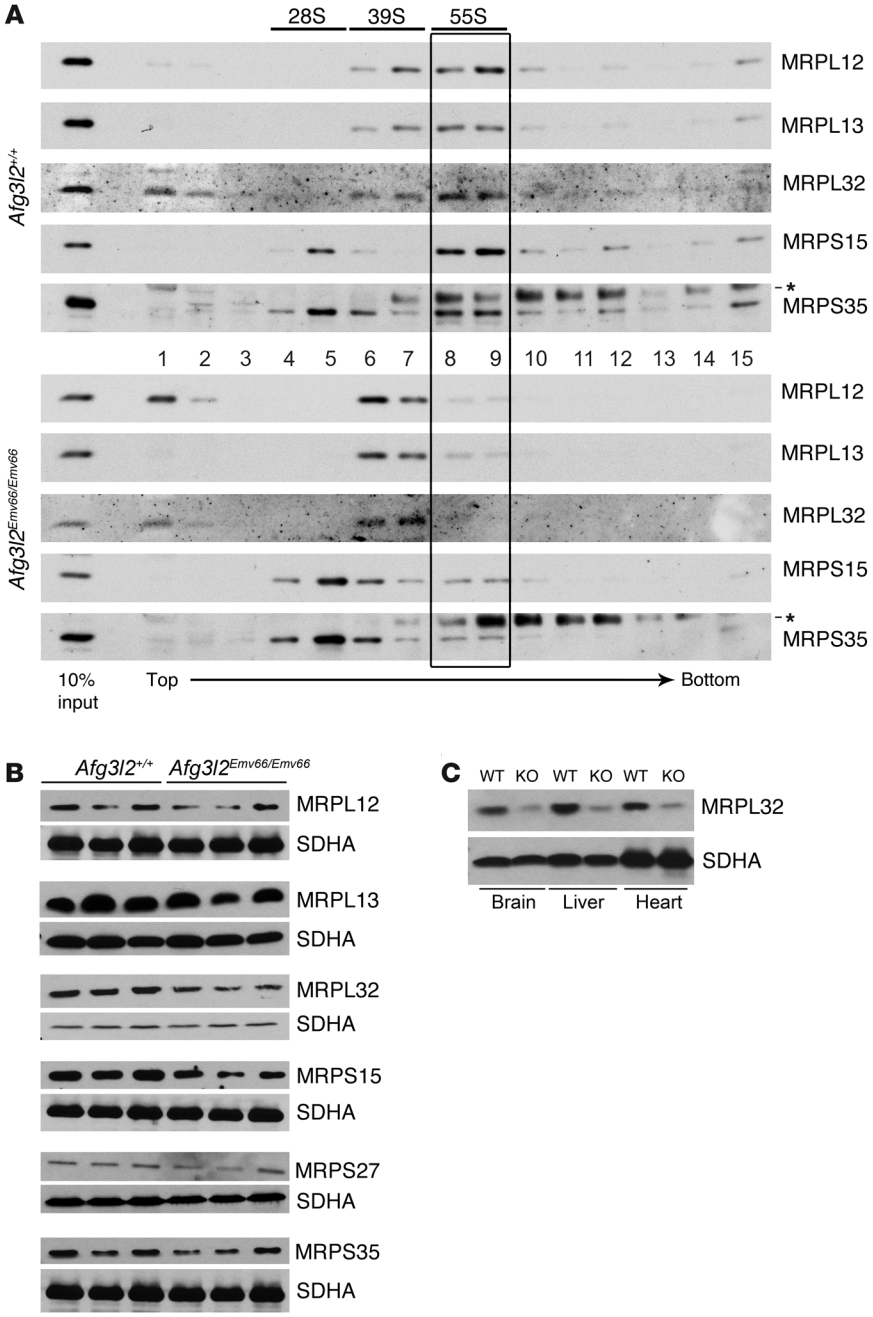

Figure 7
Impaired mitoribosome assembly in *Afg3l2*$^{Emv66/Emv66}$ mice. (**A**) The mitoribosome profile shows a clear shift to less dense fractions in the pattern of large ribosomal subunits in brain mitochondria of *Afg3l2*$^{Emv66/Emv66}$ mice when compared with those of the control *Afg3l2*$^{+/+}$ mice and reduced levels of assembled mitoribosomes (55S, boxed area). Asterisks indicate unspecific signals. (**B**) Steady-state levels of mitochondrial ribosomal proteins in the brains of *Afg3l2*$^{Emv66/Emv66}$ and *Afg3l2*$^{+/+}$ mice. The levels of MRPL32 are reduced in the *Afg3l2*$^{Emv66/Emv66}$ mice. The SDHA subunit of complex II was used as loading control. (**C**) MRPL32 levels are affected in several tissues from *Afg3l2*$^{Emv66/Emv66}$ mice as compared with those in control *Afg3l2*$^{+/+}$ mice. The SDHA subunit of complex II was used as loading control. Notably, the reduction in the levels of MRPL32 seems to be more or less pronounced depending on the mouse analyzed (compare **B** and **C**).

translation defect provides an explanation for the COX deficiency with normal SDH activity in PCs in *Afg3l2*$^{PC-KO}$ mice and for the reduced levels of assembled respiratory complex I, III, and IV (13). Our findings thus highlight the dual activity of AFG3L2 as a quality control and regulatory enzyme, which is consistent with previous studies on the yeast *m*-AAA protease. While protein synthesis is impaired in the brain in the absence of AFG3L2, partial down-regulation of *Afg3l2* in cell lines does not interfere with protein synthesis but increases the stability of some newly synthesized mt-encoded subunits of the respiratory complexes (5).

AFG3L2 supports mitochondrial translation by affecting the biogenesis of the mt-LSU and the assembly of the mitoribosome. Currently, very little is known about how assembly of mitoribosomes is achieved, and only a few factors have been identified, which are involved in the assembly of the mt-SSU or mt-LSU (34–41). Whether AFG3L2 is promoting ribosome formation or stability is at present still unclear. The protease might have a direct role or might act through maturation of one or more specific substrates. We have shown that *Afg3l2*-deficient mitochondria contain reduced levels of mature MRPL32, a known substrate of the yeast *m*-AAA protease (6), while the steady-state levels of other mitochondrial ribosomal proteins appeared largely unaffected. In yeast, processing of MRPL32 occurs close to the membrane and is required for late assembly of the mitoribosomes (6). MRPL32 maturation represents a central function of the protease in yeast and accounts for the respiratory deficiencies associated with its

loss (6). Impaired maturation of MRPL32 may therefore contribute to the defective biogenesis of the mt-LSU. However, further experiments are required to ascertain the relevance of this process, since mammalian tissues deficient of AFG3L2 do not show an accumulation of the precursor of MRPL32 and display residual levels of the mature protein, suggesting that other proteases can partially compensate.

Remarkably, we detected defects in mitochondrial translation and assembly of mitoribosomes both in brains and livers of *Afg3l2*$^{Emv66/Emv66}$ mice, indicating that regulation of mitochondrial translation is a conserved function of AFG3L2 in various tissues. The strict dependence on oxidative respiration and the high-energy requirements of specialized neuronal subcompartments may explain why neurons are exquisitely affected by lack of AFG3L2. Other predominant glycolytic tissues, such as the liver, might in fact cope with the same biochemical defect. Despite the fact that the liver does not show overt mitochondrial pathology in *Afg3l2*$^{Emv66/Emv66}$ mice (13), we cannot exclude that a hepatic phenotype might manifest if these mice lived longer. A liver-specific deletion of *Afg3l2* will help clarify this issue. Previously, we found reduced mitochondrial translation in the livers of *Spg7*$^{-/-}$ mice (6) but not in the brains (our unpublished observations). These data strongly suggest that the extent of detectable impairment of mitochondrial translation in a given tissue in different *m*-AAA protease mouse models might depend on the residual levels of *m*-AAA protease isoenzymes.

In recent years, several mutations in mitochondrial translation factors, in components of the mitoribosomes, in mitochondrial aminoacyl-tRNA synthetases, or in translational activators have been linked to human diseases (42). A variety of clinical phenotypes have been associated with these mutations, but in several cases the patients show encephalopathy or Leigh disease, highlighting again the susceptibility of the brain to defects in mitochondrial protein translation (43). Recently, mutations in the mitochondrial methionyl-tRNA synthetase have been found in patients affected by a recessive form of ataxia (44). We now propose that neurodegenerative diseases linked to *AFG3L2* mutations should also be regarded as examples of conditions associated with impaired mitochondrial protein synthesis.

Methods

Generation of Afg3l2^{PC-KO} *mice and animal experimentation*. Conditional *Afg3l2*$^{fl/+}$ mice were commercially generated at TaconicArtemis on C57BL/6 background (see Supplemental Figure 1). *Afg3l2*$^{fl/fl}$ mice were crossed with L7-Cre mice (17) to generate *Afg3l2*$^{PC-KO}$ mice. Generation of ROSA26$^{+/SmY}$ mice was previously reported (18). The *Afg3l2*$^{Emv66/Emv66}$ model was previously described (13). *Afg3l2*$^{Emv66/Emv66}$ mice analyzed in this study were obtained by breeding heterozygous mice in a mixed FVB-C57BL/6 background. The general health status of the mice was monitored regularly and assessed by the following criteria: body weight, posture, signs of pain, distress or discomfort, and insufficient grooming.

Histology, immunohistochemistry, and immunofluorescence. Mice were anesthetized with avertin and perfused intracardially with 4% paraformaldehyde in PBS. Cerebella were removed, postfixed overnight with 4% paraformaldehyde in PBS, and conserved in 0.12 M phosphate buffer. Immunohistochemistry and immunofluorescence were performed on 30-μm sagittal vibratome sections, as previously described (12). The sections were incubated with anti-calbindin antibodies (monoclonal or polyclonal, SWANT), anti-GFAP antibodies (NeoMarkers), and anti-IBA1 antibody (WAKO). Secondary antibodies used were anti-mouse Alexa Fluor 488 and Alexa Fluor 546 (Invitrogen) and anti-rabbit Alexa Fluor 546 (Invitrogen). Samples were mounted using FluorSave Reagent (Calbiochem). All immunohistochemical and immunofluorescence analyses were performed on at least 3 mice per genotype. Fluorescent images were acquired using an Axio-Imager M2 microscope equipped with Apotome 2 (Zeiss). Photographs show projected images of individual Z-stacks.

Neuropathology and ultrastructural analysis. 4-week-old wild-type and *Afg3l2*$^{PC-KO}$ mice (at least $n = 3$ for each genotype) were anesthetized intraperitoneally with avertin and perfused with 2% glutaraldehyde in PBS. Cerebella were removed and postfixed in 0.12 M phosphate buffer/2% glutaraldehyde. After treatment with osmium tetroxide, brains were embedded in Epon (Fluka). For ultrastructural analyses, blocks of tissue were selected for electron microscopy after examination of semithin sections by light microscopy. Ultrathin sections (70 nm) were cut, collected on 200 mesh copper grids (Electron Microscopy Sciences), and stained with uranium acetate (Plano GMBH) and lead citrate (Electron Microscopy Sciences).

Histochemical stainings. Frozen cerebellar cryosections were thawed and incubated in COX staining solution (DAB, cytochrome *c*, sucrose, catalase, phosphate buffer, pH 7.4) for 15 minutes and then in SDH staining solution (succinic acid, phosphate buffer, pH 7.4) for 90 minutes in a humid chamber at 37°C. Slides were washed 3 times with water for 5 minutes. Samples were dehydrated in increasing concentrations of ethanol: 90% EtOH for 1 minute, 95% EtOH for 1 minute, and 100% EtOH for 1 minute. Subsequently, the sections were washed 2 times in xylol, for 2 minutes each, and finally mounted in mounting medium.

Electrophysiology. Experiments were performed on brain slices from 4- to 5-week-old female and male *Afg3l2*$^{PC-KO}$ mice (*Afg3l2*$^{fl/fl}$;L7-Cre;ROSA26$^{+/SmY}$ mice) and their control littermates (*Afg3l2*$^{+/+}$;L7-Cre;ROSA26$^{+/SmY}$ or *Afg3l2*$^{+/-}$;L7-Cre;ROSA26$^{+/SmY}$ mice). Detailed experimental procedures are described in the Supplemental Methods.

Real-time quantification of mtDNA. Total DNA was isolated from brains of P10–P12 mice using standard techniques. Real-time amplification was performed using SYBR Green PCR Master Mix (Applied Biosystem), as previously described (12). Three mice per genotype were used.

Northern blot analysis. RNA was isolated from the brains of P10–P12 mice using the ToTally RNA Kit (Ambion). 2 μg of RNA were denatured in Glioxal Sample Load Dye (Ambion), separated in formaldehyde-containing agarose gels, and transferred to Hybond-XL membranes (GE Healthcare). DNA probes were radiolabeled with α-^{32}P-dGTP using the Random Primers DNA Labeling System (Invitrogen). Regions of the mouse mitochondrial genome (NC_005089.1) were used as probes for *Cox1* (nucleotides 5,380–6,208), *Cox3* (nucleotides 8,733–9,266), *Nd1* (nucleotides 2,822–3,332), *Cytb* (nucleotides 14,651–15,184), and *Rnr2* (nucleotides 1,749–2,172). The probe for *Rn18s* spans nucleotides 4,074–4,702 of the 45S pre RNA transcript (NR_046233.1).

Western blot analysis. Western blot analysis was performed on 40 μg of mitochondria isolated from the brain. The immunodetection of respiratory complexes subunits was performed using antibodies from Molecular Probes, Invitrogen. The MRPL12 antibody was purchased from Abcam, and the MRPS27 and MRPS35 antibodies were acquired from Protein Tech. Polyclonal antibodies against MRPL13 and MRPS15 were previously described (34, 35). Anti-mouse MRPL32 antibody was developed by using the synthetic peptide CYTGEKPSEKDQGKR to immunize rabbits (Biogenes).

In organello translation. Mitochondria from the brains of P10–P12 mice were isolated using MOPS sucrose buffer (440 mM sucrose, 20 mM MOPS, 1 mM EDTA, 0.2 mM phenylmethylsulfonyl fluoride), as previously described (12). In vitro protein synthesis was performed essentially as previously described (45), with slight modifications. Mitochondria were

incubated for 1 hour at 37°C in translation buffer containing all amino acids at a concentration of 60 μg/ml minus methionine, which was added as L-^{35}S-Methionine (GE Healthcare) at a concentration of 0.5 mCi/ml. Mitochondria were pelleted and resuspended in SDS-PAGE loading buffer.

Isokinetic sucrose gradient analysis of mitoribosomes. Mitochondria were isolated from indicated tissues (see the legends for Figure 7 and Supplemental Figure 5) using the MOPS sucrose buffer without addition of EDTA. Sucrose gradients were performed as described by Metodiev et al. (34). Briefly, 1.2 mg of mitochondria were lysed in 120 μl buffer containing 1% Triton X-100, 260 mM sucrose, 100 mM KCl, 20 mM $MgCl_2$, 10 mM Tris-HCl (pH 7.5), EDTA-free complete protease inhibitor (Roche), and 0.08 U/ml RNAsin (Promega). Mitochondrial lysates were incubated on ice for 20 minutes prior to centrifugation at 9,200 *g* for 45 minutes at 4°C. Cleared lysates (100 μl) were loaded on top of a 10% to 30% linear sucrose gradient. Sucrose gradients, containing 100 mM KCl, 20 mM $MgCl_2$, 10 mM Tris-HCl (pH 7.5), and EDTA-free complete protease inhibitor (Roche), were prepared in 14- × 89-mm centrifuge tubes (Beckman) using a Gradient Master (BioComp Instruments). After centrifugation at 71,000 *g* for 15 hours at 4°C, gradient fractions (750 μl) were collected from top to bottom, TCA precipitated, and subjected to Western blot analysis.

Statistics. Two-tailed Student's *t* test was applied for statistical analysis. *P* values below 0.01 were considered significant.

Study approval. All animal procedures were conducted in accordance with European (EU directive 86/609/EEC), national (TierSchG), and institutional guidelines and were approved by local governmental authorities (Landesamt für Natur, Umwelt und Verbraucherschutz Nordrhein-Westfalen) under the license 87–51.04.2010.A219.

Acknowledgments

We are grateful to Alexandra Kukat and Julia Harmel for help with experiments and to Helmut Wratil for excellent technical assistance. We would like to thank Carsten Merkwirth for β-galactosidase stainings in L7-Cre;Rosa26-βgal mice. This work was supported by a grant from the Deutsche Forschungsgemeinschaft (RU1653/1-1 to E.I. Rugarli; FOR885 and SFB635 to T. Langer) and from the European Research Council (ERC-Ad-233078 to T. Langer).

Received for publication May 3, 2012, and accepted in revised form August 13, 2012.

Address correspondence to: Elena I. Rugarli, Biocenter, University of Cologne, Zülpicher Str. 47b, 50674 Köln, Germany. Phone: 49.221.470.8290; Fax: 49.221.470.8590; E-mail: Elena.Rugarli@uni-koeln.de.

1. Rugarli EI, Langer T. Mitochondrial quality control: a matter of life and death for neurons. *EMBO J*. 2012;31(6):1336–1349.
2. Arlt H, Tauer R, Feldmann H, Neupert W, Langer T. The YTA10-12 complex, an AAA protease with chaperone-like activity in the inner membrane of mitochondria. *Cell*. 1996;85(6):875–885.
3. Lee S, Augustin S, Tatsuta T, Gerdes F, Langer T, Tsai FT. Electron cryomicroscopy structure of a membrane-anchored mitochondrial AAA protease. *J Biol Chem*. 2011;286(6):4404–4411.
4. Leonhard K, Guiard B, Pellecchia G, Tzagoloff A, Neupert W, Langer T. Membrane protein degradation by AAA proteases in mitochondria: extraction of substrates from either membrane surface. *Mol Cell*. 2000;5(4):629–638.
5. Hornig-Do HT, et al. Nonsense mutations in the COX1 subunit impair the stability of respiratory chain complexes rather than their assembly. *EMBO J*. 2012;31(5):1293–1307.
6. Nolden M, Ehses S, Koppen M, Bernacchia A, Rugarli EI, Langer T. The m-AAA protease defective in hereditary spastic paraplegia controls ribosome assembly in mitochondria. *Cell*. 2005;123(2):277–289.
7. Atorino L, et al. Loss of m-AAA protease in mitochondria causes complex I deficiency and increased sensitivity to oxidative stress in hereditary spastic paraplegia. *J Cell Biol*. 2003;163(4):777–787.
8. Koppen M, Metodiev MD, Casari G, Rugarli EI, Langer T. Variable and tissue-specific subunit composition of mitochondrial *m*-AAA protease complexes linked to hereditary spastic paraplegia. *Mol Cell Biol*. 2007;27(2):758–767.
9. Di Bella D, et al. Mutations in the mitochondrial protease gene AFG3L2 cause dominant hereditary ataxia SCA28. *Nat Genet*. 2010;42(4):313–321.
10. Pierson TM, et al. Whole-exome sequencing identifies homozygous AFG3L2 mutations in a spastic ataxia-neuropathy syndrome linked to mitochondrial *m*-AAA proteases. *PLoS Genet*. 2011;7(10):e1002325.
11. Casari G, et al. Spastic paraplegia and OXPHOS impairment caused by mutations in paraplegin, a nuclear-encoded mitochondrial metalloprotease. *Cell*. 1998;93(6):973–983.
12. Martinelli P, et al. Genetic interaction between the *m*-AAA protease isoenzymes reveals novel roles in cerebellar degeneration. *Hum Mol Genet*. 2009;18(11):2001–2013.
13. Maltecca F, et al. The mitochondrial protease AFG3L2 is essential for axonal development. *J Neurosci*. 2008;28(11):2827–2836.
14. Maltecca F, Magnoni R, Cerri F, Cox GA, Quattrini A, Casari G. Haploinsufficiency of AFG3L2, the gene responsible for spinocerebellar ataxia type 28, causes mitochondria-mediated Purkinje cell dark degeneration. *J Neurosci*. 2009;29(29):9244–9254.
15. Ehses S, et al. Regulation of OPA1 processing and mitochondrial fusion by m-AAA protease isoenzymes and OMA1. *J Cell Biol*. 2009;187(7):1023–1036.
16. Chen H, McCaffery JM, Chan DC. Mitochondrial fusion protects against neurodegeneration in the cerebellum. *Cell*. 2007;130(3):548–562.
17. Barski JJ, Dethleffsen K, Meyer M. Cre recombinase expression in cerebellar Purkinje cells. *Genesis*. 2000;28(3-4):93–98.
18. Sterky FH, Lee S, Wibom R, Olson L, Larsson NG. Impaired mitochondrial transport and Parkin-independent degeneration of respiratory chain-deficient dopamine neurons in vivo. *Proc Natl Acad Sci U S A*. 2011;108(31):12937–12942.
19. Chiesa N, Barlow C, Wynshaw-Boris A, Strata P, Tempia F. Atm-deficient mice Purkinje cells show age-dependent defects in calcium spike bursts and calcium currents. *Neuroscience*. 2000;96(3):575–583.
20. Inoue T, Lin X, Kohlmeier KA, Orr HT, Zoghbi HY, Ross WN. Calcium dynamics and electrophysiological properties of cerebellar Purkinje cells in SCA1 transgenic mice. *J Neurophysiol*. 2001;85(4):1750–1760.
21. McKay BE, et al. Climbing fiber discharge regulates cerebellar functions by controlling the intrinsic characteristics of purkinje cell output. *J Neurophysiol*. 2007;97(4):2590–2604.
22. Nelson TE, Campbell IL, Gruol DL. Altered physiology of Purkinje neurons in cerebellar slices from transgenic mice with chronic central nervous system expression of interleukin-6. *Neuroscience*. 1999;89(1):127–136.
23. Servais L, Hourez R, Bearzatto B, Gall D, Schiffmann SN, Cheron G. Purkinje cell dysfunction and alteration of long-term synaptic plasticity in fetal alcohol syndrome. *Proc Natl Acad Sci U S A*. 2007;104(23):9858–9863.
24. Womack M, Khodakhah K. Active contribution of dendrites to the tonic and trimodal patterns of activity in cerebellar Purkinje neurons. *J Neurosci*. 2002;22(24):10603–10612.
25. Ishihara N, Fujita Y, Oka T, Mihara K. Regulation of mitochondrial morphology through proteolytic cleavage of OPA1. *EMBO J*. 2006;25(13):2966–2977.
26. Duvezin-Caubet S, et al. Proteolytic processing of OPA1 links mitochondrial dysfunction to alterations in mitochondrial morphology. *J Biol Chem*. 2006;281(49):37972–37979.
27. Head B, Griparic L, Amiri M, Gandre-Babbe S, van der Bliek AM. Inducible proteolytic inactivation of OPA1 mediated by the OMA1 protease in mammalian cells. *J Cell Biol*. 2009;187(7):959–966.
28. Chakrabarti L, et al. Mitochondrial dysfunction in NnaD mutant flies and Purkinje cell degeneration mice reveals a role for Nna proteins in neuronal bioenergetics. *Neuron*. 2010;66(6):835–847.
29. Girard M, et al. Mitochondrial dysfunction and Purkinje cell loss in autosomal recessive spastic ataxia of Charlevoix-Saguenay (ARSACS). *Proc Natl Acad Sci U S A*. 2012;109(5):1661–1666.
30. Khandelwal PJ, Herman AM, Moussa CE. Inflammation in the early stages of neurodegenerative pathology. *J Neuroimmunol*. 2011;238(1–2):1–11.
31. Yamada K, Watanabe M. Cytodifferentiation of Bergmann glia and its relationship with Purkinje cells. *Anat Sci Int*. 2002;77(2):94–108.
32. Hanisch UK, Kettenmann H. Microglia: active sensor and versatile effector cells in the normal and pathologic brain. *Nat Neurosci*. 2007;10(11):1387–1394.
33. Viscomi C, et al. In vivo correction of COX deficiency by activation of the AMPK/PGC-1alpha axis. *Cell Metab*. 2011;14(1):80–90.
34. Metodiev MD, et al. Methylation of 12S rRNA is necessary for in vivo stability of the small subunit of the mammalian mitochondrial ribosome. *Cell Metab*. 2009;9(4):386–397.
35. Camara Y, et al. MTERF4 regulates translation by targeting the methyltransferase NSUN4 to the mammalian mitochondrial ribosome. *Cell Metab*. 2011;13(5):527–539.
36. Dennerlein S, Rozanska A, Wydro M, Chrzanowska-Lightowlers ZM, Lightowlers RN. Human ERAL1 is a mitochondrial RNA chaperone involved in the assembly of the 28S small mitochondrial ribosomal subunit. *Biochem J*. 2010;430(3):551–558.
37. He J, et al. Human C4orf14 interacts with the mitochondrial nucleoid and is involved in the biogene-

sis of the small mitochondrial ribosomal subunit. *Nucleic Acids Res*. 2012;40(13):6097–6108.
38. Kolanczyk M, et al. NOA1 is an essential GTPase required for mitochondrial protein synthesis. *Mol Biol Cell*. 2011;22(1):1–11.
39. Rorbach J, Gammage PA, Minczuk M. C7orf30 is necessary for biogenesis of the large subunit of the mitochondrial ribosome. *Nucleic Acids Res*. 2012; 40(9):4097–4109.
40. Uchiumi T, et al. ERAL1 is associated with mitochondrial ribosome and elimination of ERAL1 leads to mitochondrial dysfunction and growth retardation. *Nucleic Acids Res*. 2010;38(16):5554–5568.
41. Wanschers BF, et al. C7orf30 specifically associates with the large subunit of the mitochondrial ribosome and is involved in translation. *Nucleic Acids Res*. 2012;40(9):4040–4051.
42. Smits P, Smeitink J, van den Heuvel L. Mitochondrial translation and beyond: processes implicated in combined oxidative phosphorylation deficiencies. *J Biomed Biotechnol*. 2010;2010:737385.
43. Rotig A. Human diseases with impaired mitochondrial protein synthesis. *Biochim Biophys Acta*. 2011;1807(9):1198–1205.
44. Bayat V, et al. Mutations in the mitochondrial methionyl-tRNA synthetase cause a neurodegenerative phenotype in flies and a recessive ataxia (ARSAL) in humans. *PLoS Biol*. 2012;10(3):e1001288.
45. Cote C, Poirier J, and Boulet D. Expression of the mammalian mitochondrial genome. Stability of mitochondrial translation products as a function of membrane potential. *J Biol Chem*. 1989; 264(15):8487–8490.